A new lithium-ion battery using 3D-array nanostructured graphene-sulfur cathode and silicon oxide-based anode

Almudena Benítez[a], Daniele Di Lecce[b], Giuseppe Antonio Elia[c], Álvaro Caballero[a], Julián Morales[*,a], and Jusef Hassoun[*,b]

[a]Dpto. Química Inorgánica e Ingeniería Química, Instituto de Química Fina y Nanoquímica, Universidad de Córdoba, 14071 Córdoba, Spain.

[b]Department of Chemical and Pharmaceutical Sciences, University of Ferrara, Via Fossato di Mortara, 17, 44121, Ferrara, Italy.

[c]Technische Universität Berlin, Research Center of Microperipheric Technologies, Gustav-Meyer-Allee 25, 13355 Berlin, Germany.

*Corresponding authors:

e-mail addresses: iq1mopaj@uco.es (J. Morales), jusef.hassoun@unife.it (J. Hassoun).

Abstract

In this work we report an efficient lithium-ion battery using enhanced sulfur-based cathode and silicon oxide-based anode as novel energy-storage system. The sulfur-carbon composite, exploiting graphene carbon with 3D array (3DG-S), is synthesized by reduction step and microwave-assisted solvothermal technique and fully characterized in terms of structure, morphology, thereby revealing suitable features for lithium-cell application. Electrochemical tests indicate the 3DG-S electrode as very stable and performing cathode in lithium half-cell, with capacity ranging from 1200 to 1000 mAh g^{-1} at C/10 and 1C rates, respectively. Remarkably, the Li-alloying anode, namely a Li_ySiO_x-C prepared by the sol-gel method and lithiated by surface treatment, shows a suitable performance in lithium half-cell using an electrolyte designed for lithium-sulfur battery. The Li_ySiO_x-C/3DG-S battery reveals very promising results with a capacity of about 460 mAh g_S^{-1} delivered at average voltage of

about 1.5 V over 200 cycles, suggesting the characterized materials as suitable candidates for low-cost and high-energy storage application.

Keywords: 3D-graphene; sulfur; solvothermal-microwave; silicon, Li-ion battery.

1. Introduction

Among the most abundant elements on the earth crust, sulfur and carbon represent very suitable candidates as electrode material for new-generation energy-storage devices based on lithium conversion reaction.[1] High energy and low cost are very attracting characteristics which, in principle, make sulfur an actual alternative for lithium-insertion cathodes used in the most conventional and nowadays the most diffused lithium-ion battery (LIB).[2] The latter system, well optimized and efficient, has a maximum energy density of about 250 Wh kg^{-1},[3] while lithium cells based on sulfur may theoretically reach a value higher than 1200 Wh kg^{-1}[4] which is well suitable for application in emerging and attractive field such as electric vehicles.[5] Despite the remarkable potentiality, sulfur suffers in lithium cell from several drawbacks, such as low conductivity, reflecting into high polarization, and the formation of soluble species, i.e., Li_2S_8 and Li_2S_6 polysulfides,[6] which react with the conventional electrolytes and, at the same time, migrate to the lithium anode leading to a "shuttle reaction" strongly affecting the cell efficiency and cycle life.[7] Furthermore, the reaction of sulfur with lithium may proceed by the formation of insoluble and insulating species (Li_2S_4, Li_2S_2 and Li_2S) which precipitate at the electrode/electrolyte interface leading to active mass loss, increased polarization and finally to cell failure.[8] These issues may be mitigated by the preparation of composite sulfur materials including carbon nano-spherules,[9] nano-sheets,[10] nano-tubes,[11] graphene,[12] and other nanostructured inactive supports.[13,14] In addition, the use of electrolytes characterized by low reactivity against lithium and polysulfides, high conductivity, and relevant safety represents a further improvement of the lithium-sulfur cell suitable for increasing cycle life, efficiency and reliability.[15–17] Ethers, glymes,[18] and

poly(ethylene oxide),[19] are very promising solvents for achieving high-performance lithium-sulfur cell, while lithium trifluorosulfonimmide (LiTFSI) and lithium trifluoromethansulfonate ($LiCF_3SO_3$) show the best characteristics as the electrolyte salts in terms of fast Li-ion transport and high conductivity.[15]

Despite the appealing features of the Li/S battery in terms of cost, environmental impact and performance, its commercialization has been limited so far owing to issues related to the lithium-metal anode. Indeed, the use of lithium metal at the negative side may lead to safety issue associated with possible lithium dendrite growth, short circuit and thermal runaway.[3] Therefore, the lithium-ion configuration may improve the cell cycle life, and performances by avoiding the lithium dendrite formation and by decreasing the interfacial resistance, thereby increasing the cell reliability.[20] Indeed, the lithium-ion anodes are typically characterized by a higher chemical stability than the lithium-metal electrode, yielding to high-energy, safe, and low-cost lithium-ion sulfur cells.[3] Accordingly, safety and stability of the sulfur cell may be increased by replacing the lithium-metal anode by graphite,[21,22] amorphous carbons[23] and lithium-alloying materials.[19,24] Following this trend, we report in this study a new promising battery formed by combining a sulfur-3D graphene composite cathode and a nanostructured silicon-carbon anode. The lithium-ion sulfur cell is investigated in terms of electrochemical characteristics in view of possible use as an advanced system for high energy storage application.

2. Experimental

2.1. Synthesis of graphite oxide

Graphite oxide (GO) was prepared by modified Hummers method.[25] In a typical synthesis, 3 g of graphite powder (Merck), 70 mL of H_2SO_4 (98 %, Panreac), and 1.5 g of $NaNO_3$ (Sigma Aldrich) were added into a 1 L flask in an ice-water bath under continuous stirring. After 20

min, 9 g of $KMnO_4$ (Sigma Aldrich) were slowly added to keep the temperature of the suspension lower than 20 ºC. Then, the reaction system was transferred to a 35 ± 5 ºC water bath and stirred for about 30 min until formation of a thick paste. Afterwards, the solution was added by 140 ml of deionized water, and stirred for 15 min at 90 ± 5 ºC before adding further 500 ml of water. Subsequently, an amount of 15 ml of H_2O_2 (3 %, Sigma Aldrich) was slowly added until formation of a dark brown gel, which was filtered, centrifugated, and washed with 250 ml of a 10 % aqueous solution of HCl (37 %, Panreac), and with water to reach a neutral pH. GO was finally obtained drying at 60 ºC into an oven during 12 h.

2.2. Synthesis of 3D graphene (3DG)

A solvothermal technique was used to exfoliate and reduce the graphite oxide in one step under microwave irradiation (Milestone flexiWAVE). In detail, an amount of 40 ml of GO aqueous suspension (2 mg ml^{-1}) was dispersed using ultrasonication for 1 h. Then, the solution was transferred into a 100-ml Teflon-lined autoclave, and put into a microwave oven at power of 350 W, and temperature of 200 ºC for 6 h to form a carbon monolith. After cooling, the monolith was filtered, and washed with distilled water. The obtained hydrogel was cooled at – 80 ºC, and dried in a freeze dryer (Telstar LyoQuest, Mod. 85). Hereafter, the sample is named 3DG.

2.3. Preparation of 3D graphene–sulfur composite (3DG-S)

The 3DG sample was mixed with 100 ml of deionized water and 10 ml of dry absolute ethanol (Panreac), and then sonicated for 30 min to get a dispersion. An amount of 200 mg of sublimed sulfur (VWR Chemical) was added into 10 ml of ethylenediamine anhydrous (Sigma Aldrich) to form a sulfur-amine precursor solution, which was then dropwise added into the 3DG dispersion within 3 min under magnetic stirring.[26] The mixed solution was

continuously stirred for 10 min, and then the final product (indicated by 3DG-S) was obtained through filtration, rinsing and drying at 50 °C.

2.4. Preparation of SiO_x-based composite

The SiO_x-based composite was prepared by sol-gel approach.[27] 18 g of resorcinol and 58.5 g of formaldehyde were mixed until a homogenous solution was obtained. An amount of 21 g of tetraethyl orthosilicate (TEOS) was added to the solution, which was then heated at 70 °C. The heated solution was then added dropwise by 2 ml of a 1M HCl aqueous solution to catalyze the formation of a pink semitransparent homogeneous gel. After aging for 24 hours at room temperature, the gel was cut into pieces, washed with ethanol, and annealed at 1000 °C for 10 h under a Ar-H_2 (5%) flow to obtain a black powder, which was grinded into a mortar.[27]

2.5. Characterization of 3D graphene and composite

X-ray diffraction (XRD) patterns were recorded either with a Bruker D8 Discover X-ray diffractometer using a Cu Kα radiation and a Ge monochromator for the GO sample or a Bruker D8 Advance diffractometer equipped using a Cu Kα radiation and a graphite monochromator for the 3DG and 3DG-S samples. The XRD analyses were performed within the 5 – 80º (2θ) range, with a step size of 0.015º and 0.1 s per step. Raman measurements were carried out through a Renishow inVida Microscope equipped with a detector Renishaw CCD Camera (578 x 400), and a laser of 532 nm edge in line focus mode. The sulfur content was determined by thermogravimetric analysis (TGA) through a Mettler Toledo-TGA/DSC under nitrogen atmosphere in the temperature range from 25 to 600 ºC using a ramp rate of 5 ºC min^{-1}. Samples morphology was investigated with a Jeol JSM-7800F and a Zeiss EVO 40 scanning electron microscopes (SEMs). SEM-EDX studies were performed by using the latter microscope equipped with a X-ACT Cambridge Instrument analyzer. Carbon,

hydrogen, nitrogen, and sulfur (CHNS) elemental analysis was carried out by EuroVector EA-3000. X-ray photoemission spectroscopy (XPS) was obtained by a Physical Electronics PHI 5700 spectrometer, using monochromatic Mg K_α radiation, and a multichannel detector. All spectra were fitted to Gauss–Lorentz curves in order to better identify the different functional group in each material. Specific surface area was determined with a Quantachrome Instruments Autosorb iQ/ASiQwin, using N_2 gas as adsorbate. Pore size distribution was calculated by the density functional theory (DFT) method applied to the adsorption branch of the isotherms.

2.6. Electrodes preparation

The negative and the positive electrodes were prepared by mixing the active material with PVDF (6020, binder, Solvay) and Super P carbon (conducting agent, Timcal) in the weight ratio of 8:1:1, and adding 1-methyl-2-pyrrolidone (NMP, Sigma Aldrich) as the solvent. The resulting anode and cathode slurries were cast on either copper (MTI) or carbon cloth (GDL ELAT LT1400) supports, respectively, through a doctor blade (MTI). The electrode foils were dried for 3 hours at 70 °C by using a hot-plate, and cut into 14-mm disks (1.54 cm^2 geometric surface). The anode and cathode disks were dried under vacuum at 110 ºC and at 45 ºC, respectively. The active material loading was 2.4 mg cm^{-2} for the anode and between 1.4 and 2.2 mg_S cm^{-2} for the cathode. A further 3DG-S composite electrode with high sulfur loading of 4.0 mg_S cm^{-2} was prepared (see the Supplementary Information for further details). Prior to use, the SiO_x-C electrode was chemically pre-lithiated (Li_ySiO_x-C) by surface treatment inside an Ar-filled glovebox (H_2O and O_2 content lower than 1 ppm).[28] The electrode disk was placed in contact with a Li foil wet by a 1 M solution of $LiPF_6$ in ethylene carbonate/dimethyl carbonate (EC:DMC; 1:1 w/w; LP30, battery grade, BASF) and pressed at 2 kg cm^{-2} for 3 hours; afterwards, the electrode was washed with DOL and used.

2.7. Electrochemical measurements

CR2032 coin-cells (MTI) were assembled inside an Ar-filled glovebox (MBraun, H_2O and O_2 content lower than 1 ppm) by stacking anode, polyethylene (Celgard) separator soaked by 30-80 µl of the electrolyte and cathode. A solution formed by dissolving 1 mol of LiTFSI (Sigma Aldrich), and 1 mol of $LiNO_3$ (Sigma Aldrich) in 1 kg a of a 1:1(w:w) mixture of 1,3-dioxolane (DOL, Sigma Aldrich) and 1,2-dimethoxyethane (DME, Sigma Aldrich) was used as the electrolyte in all the electrochemical tests. Lithium metal disks were used as the anode for the tests in lithium-half cell. Cyclic voltammetry (CV) measurements were performed at a scan rate of 0.1 mV s^{-1} by using a VersaSTAT MC Princeton Applied Research (PAR) analyzer. CV tests were carried out within the 1.8– 2.8 V range for the 3DG-S electrode, and within the 0.01 – 2.8 V range for the Li_ySiO_x-C one (see the Supplementary Information for further details). Electrochemical impedance spectroscopy (EIS) measurements were performed by means of the same instrument during the CV scans, by applying to the cells a 10 mV alternate signal between the 500 kHz – 0.1 Hz frequency range. Nonlinear least squares (NLLS) analysis of the EIS data were carried out by means of the Boukamp package.[29] Galvanostatic cycling measurements were carried out through a MACCOR series 4000 battery test system. All the capacity values have been calculated considering the sulfur mass and indicated in mAh g_S^{-1}. Rate capability galvanostatic tests of Li/3DG-S cells (using both low and high S loading; see the Supplementary Information for further details) were performed at C/10, C/8, C/5, C/3, C/2 and 1C rate (1C = 1675 mA g_S^{-1}). Cycling tests of Li/3DG-S cells were also performed at constant currents of C/3, C/2, and 1C rates (1C = 1675 mA g_S^{-1}) over 100 cycles. All the cycling tests in lithium half-cell of the 3DG-S electrode were carried out within 1.9 – 2.8 V range, except for the cycles at 1C rate, in which the discharge cutoff was lowered to 1.8 V. The Li_ySiO_x-C electrode was studied in lithium-half cell by galvanostatic cycling at 100 mA g^{-1} within the 0.01 – 2 V voltage range. A

lithium-ion full-cell was assembled by using a Li_ySiO_x-C anode with active material loading increased to about 5 mg cm^{-2}, and a 3DG-S cathode with sulfur loading decreased to about 1 mg cm^{-2}, to obtain a negative-to-positive ratio of 1.07 taking into account a maximum cathode capacity of 1350 mAh g_S^{-1} and a maximum anode capacity of 290 mAh g^{-1} (see manuscript discussion). The full-cell was galvanostatically cycled at a C/5 rate with respect to the cathode (1C = 1675 mA g_S^{-1}) within the 0.8 – 2.4 V voltage range. All the electrochemical tests were performed at 23 °C. A scheme of the new full lithium-ion sulfur cell coupling the silicon oxide-based anode and the 3DG-S composite cathode is reported in Fig. 1. The figure elucidates the electrochemical alloying process at the silicon oxide-based anode and the conversion reaction of the sulfur-based cathode studied in this work.

Figure 1

3. Results and Discussion

Structural, morphological and textural properties of the sulfur-based cathode material are following reported (Figure 2), while those of the SiO_x-based anode may be found in our previous paper.[27] Fig. 2a shows the XRD patterns of GO, 3DG and 3DG-S, as well as the reference patterns of crystalline sulfur (PDF # 85-0799) and graphite (PDF # 75-1621). The XRD pattern of GO (bottom pattern in Fig. 2a) reveals the (001) peak at $2\theta = 11.4°$ already reported by literature,[30] and the absence of peaks due to graphite phase. On the other hand, the 3DG sample (intermediate pattern in Fig. 2a) shows very broad peaks at $2\theta = 26^o$ and 44°, attributed respectively to the (002) and (100) diffractions of the *graphite-like* structure, thus suggesting high disorder in the stacking of the graphene nanosheets.[31,32]. As for the 3DG-S composite (top pattern in Fig. 2a), the XRD indicates well-defined peaks assigned to the orthorhombic sulfur polymorph (PDF # 85-0799), which almost completely mask the 3DG matrix reflections. The sulfur weight ratio in the composite was evaluated to be of the order

of 65% by TGA, as reported in Fig. S1 in the Supplementary Information which shows a one-step weight loss between 150 and 300 ºC attributed to the sulfur evaporation.[9] Further details on the composite are revealed by the Raman spectra of GO and 3GD reported in Fig. 2b, which shows the D and G bands of carbon at about 1350 cm^{-1} and 1590 cm^{-1} for both samples. The characteristic intensity ratio between the D and G bands (I_D/I_G) increases from 0.90 in GO (bottom curve in Fig. 2c) to 1.01 in 3DG (top curve in Fig. 2c), thus indicating for the latter a decrease in the average size of the sp^2 domains which is in line with the XRD results.[33,34] Furthermore, the XPS analysis performed on the sample, and reported in Fig. 2c-d, allows the evaluation of the solvothermal treatment effects on the surface functional groups of the carbon matrix. The XPS spectra in the C 1s region of GO (Fig. 2c) and 3DG (Fig. 2d) have been fitted by overlapped peaks attributed respectively to the C–C bond (284.8 eV), the oxygen-carbon bonds of the hydroxyl (285.9 eV), epoxy (286.7 eV), carbonyl (288.0 eV), and carboxyl (289.0 eV) groups,[35] and to the $\pi \rightarrow \pi^*$ transition (wake-up; 290.8 eV).[36] The contribution of each component is summarized in Table 1 which reveals for 3DG a significant deoxygenation whit respect to GO. Indeed, the data indicate negligible contribution of the $\pi \rightarrow \pi^*$ and hydroxyl groups, [37–39] as well as strong signal at the binding energy of the epoxy group for GO, and by contrast, a large contribution of the C–C bond and minor surface functional groups for 3DG.

Table1

The effect of the solvothermal treatment on the surface area and pore morphology was investigated by N_2 adsorption/desorption measurements. Fig. 2e shows the related isotherms, having a type IV shape according to the BDDT classification, and suggesting monolayer-multilayer and capillary condensation due a mesoporous morphology. Despite the similar isotherm shapes, significant differences are observed in the BET surface area and pore volume values of the samples reported in Table 2. The data indicate an increase of the

estimated surface area and pore volume of 3DG sample by a factor of about 6.3 when compared to the GO one.

Table 2

In particular, the pore size distribution by DFT model of the GO and 3DG samples shown in Fig. 2f reveals for the latter mesopores of different size, mostly below 5 nm, as well as micropores of about 2 nm, while the GO shows a low porosity which is indeed expected by its low surface area. It is noteworthy herein that sulfur is expected to partially fill the pores of 3DG to enhance the cell performances of 3DG-S material, however a fraction of the active material may be actually located outside the pores as evidenced by literature.[40,41]

Figure 2

Sample morphology and elemental composition are herein detected by coupling SEM, and SEM-EDS as reported in Fig. 3. The SEM images of the GO material reported in Fig. 3a and Fig. 3b reveal a layered morphology consisting of micrometric particles with various size formed by stacked flakes. The solvothermal treatment modifies this morphology by exfoliation and assembly processes of the GO flakes, leading to a micrometric, three-dimensional network of randomly-oriented, wrinkled graphene sheets, as shown by the SEM images of 3DG in panels c, e and g of Fig. 3. Furthermore, the micrographs of the 3DG-S composite, reported in Fig 3 (d,f,h,i), suggest the presence of smooth submicrometric particles of sulfur, which are also detected by the EDS maps in Fig. 3 (l,m), within and besides the graphene sheets which partially hold the overall 3D-morphology. Therefore, we can describe the 3DG-S material as a composite formed by partially-graphitic, randomly-oriented graphene sheets, arranged into three-dimensional aggregates whose pores are filled by crystalline sulfur, which is also located over the surface of the 3DG network. As already mentioned, such structural and morphological features are expected to ensure reversible sulfur reduction at high current rate.

Figure 3

The electrochemical behavior of the 3DG-S composite in the lithium half-cell was studied by combining voltammetry, impedance spectroscopy and galvanostatic measurements. Fig. 4a shows the voltammetry profiles upon 6 cycles the lithium cell using the 3DG-S electrode. The figure clearly exhibits upon the first discharge the electrochemical response due to the formation of long-chain (i.e., Li_2S_8, Li_2S_6) and short-chain (i.e., Li_2S_4, Li_2S_2, Li_2S) polysulfides through two peaks, respectively occurring at 2.3 and 2.0 V.[17] The reverse oxidation takes place through electrochemical processes between 2.2 and 2.5 V, by two merged peaks at 2.3 and 2.4 V. The 3DG-S electrode reacts by conversion,[4] as reported below:

$$S_8 + 2\ Li^+ + 2\ e^- \rightleftarrows Li_2S_8 \quad (1)$$

$$Li_2S_8 + 14\ Li^+ + 14\ e^- \rightleftarrows 8\ Li_2S \quad (2)$$

The two voltammetry peaks during charge and discharge observed in Fig. 4a may be therefore justified by these two overall processes.

The subsequent cycles reveal a significant decrease of polarization for the first reduction step (long-chain polysulfides formation), as well as a decrease of the oxidation peak at 2.4 V. This behavior, already observed in the literature on carbon-sulfur composites,[17] is likely attributed to a decrease of the electrode/electrolyte interface resistance, according the EIS results shown in Fig. S2 of the Supplementary Information. EIS spectra have been recorded at the open circuit voltage (OCV) of the Li/3DG-S cell as well as after 6 and 11 cycles of voltammetry. The related Nyquist plots (see Fig. S2 in the Supplementary Information) suggest a significant decrease of the interface resistance associated with the electrode/electrolyte interface due to the cell cycling, as clearly indicated by the NLLS analysis[29] reported in Table S1 of the Supplementary Information. Therefore,

the CV and EIS data suggest reversible electrochemical processes with low electrode/electrolyte interface resistance. The rate capability of the cell is shown in Fig. 4b, which reveals reversible capacity of 1176, 1109, 1048, 1017, 1004, and 1001 mAh g_S^{-1} at current rates of increasing from C/10 to C/8, C/5, C/3, C/2, and 1C, respectively (1C = 1675 mA g_S^{-1}), with a Coulombic efficiency higher than 99%. Moreover, the cell exhibits the typical two-plateau voltage profile with values centered at 2.2 V and 2.3 V in agreement with CV results, and low polarization even at increased currents, as shown by Fig. S3 in the Supplementary Information. The remarkable stability of the 3DG-S material is suggested in Fig 4b by the recovery of 94% of the initial capacity by lowering back the current to C/10 at the 31st cycle. Galvanostatic tests at a constant current of C/3, C/2 and 1C, respectively, are used to check the cell performance as prolonged to 100 cycles. The related voltage profiles, shown in Fig. 4c, reveal the above mentioned two plateaus at about 2.3 V and 2.1 V upon discharge, and reversed charge plateaus at 2.2 V and 2.4 V, as well as the expected decrease of capacity, and slight increase of polarization, by raising current. Accordingly, the Li/3DG-S cell delivers a reversible capacity of 1350, 1270 and 1020 mAh g_S^{-1} upon the first cycle at C/3, C/2 and 1C rates, respectively, while the retained capacity after 100 cycles ranges from 70% to 80% of the initial value, depending on the cycling rate (Fig. 4d). Remarkably, the cell shows a Coulombic efficiency values approaching 100% after few stabilization cycles in which the solid electrolyte interface (SEI) is formed, thereby suggesting negligible shuttle-effect over the current range herein exploited. In this respect, our results are in agreement with the literature on comparable S-based materials. In particular, a graphene−sulfur−carbon nanofibers coaxial material containing 33 wt.% of S has shown a capacity of 1047 mAh g_S^{-1} at 0.1C rate, decreasing to 660 mAh g_S^{-1} after 100 cycles.[42] Morphology tailoring into graphene nanosheets entrapping sulfur with a final loading of 65 wt.% may lead to reversible capacities of 1370, 1150, and 950 mAh g_S^{-1} at current rates of C/5, C/2, and 1C,

respectively,[43] while the three-dimensional porous array of the graphene sheets may yield to carbon matrixes able to host into the pores large amount of elemental sulfur (63 and 72 wt.%), delivering a capacity ranging from 1100 to 1200 mAh g_S^{-1} at C/2 rate.[44] Moreover, a graphene foam electrode with high sulfur loading of about 10 mg cm^{-2} has demonstrated a capacity of 1000 mAh g_S^{-1} at 0.9C rate, which decreased to 450 mAh g_S^{-1} after 1000 cycles.[45] Recently, three-dimensional composite carbon-sulfur cathodes with high areal sulfur loading values of about 4 mg cm^{-2} exhibited a reversible capacity ranging from 900 to 1200 mAh g_S^{-1} at about 0.1C rate.[46,47]

Herein, we have performed further cycling tests increasing the sulfur mass loading from about 2.0 mg cm^{-2} (tests in Fig. 4) to 4.0 mg cm^{-2} (see Fig. S4 in Supplementary Information). Fig. S4 reveals only minor effects on the performance due to the loading increase, both in terms of voltage profiles (panel a) and cycling behavior (panel b), *i.e.*, capacity from 1100 to 950 mAh g^{-1} within the current rate range between C/10 and C/2. Despite the significant polarization observed at 1C rate, due to the relevant loading, it may be pointed out that the cell may still deliver about 800 mAh g_S^{-1}, thus suggesting the 3DG-S composite as a promising electrode material for lithium-sulfur cell. The cell recovers a capacity of 1050 mAh g^{-1} as the current is lowered back to C/10 at the 31st cycle (Fig. S4b), thus indicating remarkable stability.

The relevant rate performance of the 3DG-S electrode has been further demonstrated by increasing the sulfur mass loading from about 2.0 mg cm^{-2} (tests in Fig. 4) to 4.0 mg cm^{-2} (test in Fig. S4 in Supplementary Information). Indeed, Fig. S4 reveals only minor effects on the performance due to the loading increase within the current rate range between C/10 and C/2, both in terms of voltage profiles (panel a) and cycling behavior (panel b). Despite the significant polarization observed at 1C rate, due to the relevant loading, it may be pointed out

that the cell may still deliver about 800 mAh g_S^{-1}, thus suggesting the 3DG-S composite as a promising electrode material for lithium-sulfur cell.

Figure 4

The study herein reported belongs to a line of research, carried out in our laboratory, focusing on full lithium-ion cells that employ S-based cathodes. Accordingly, we have systematically investigated in recent literature papers the Li-ion cell characteristics by varying the electrode and electrolyte components.[19,20,22,24,48–51] Such incremental studies have surveyed the possibility of using sulfur-carbon, and Li_2S-carbon composites in lithium-ion cells with liquid, gel, and polymer electrolytes, previously consisting of polyethylene oxide-alkyl carbonates mixtures,[48,49] and lately based on ether solvents dissolving polysulfides.[20,22] As for the lithium-ion anode, we have already investigated alloy-carbon electrodes based on tin[19,48,49,51] and silicon[20,24,50] as well as conventional graphite.[22] Therefore, we successfully improved the Li-ion sulfur battery performance in terms of both reversible capacity and cycling behavior since the first works by optimizing the cell configuration.[19,20,22,24,48–51]

The 3DG-S electrode is therefore studied in a new lithium-ion battery employing a SiO_x-C anode, characterized in our previous work using conventional carbonate electrolyte. Herein, we extend the study in an electrolyte designed for lithium sulfur battery, that is, based on DOL, DME, LiTFSI, and $LiNO_3$, and adopting a lithiated configuration of the material (Li_ySiO_x-C), which has been obtained by chemical treatment with lithium of the electrode before use in cell (see the Experimental section for further details). This procedure, developed in our previous study,[28] allows the anode to act as a lithium reservoir in an electrochemical system using a delithiated cathode, and leads to efficient operation of the sulfur electrode in a metal free, lithium-ion configuration as demonstrated in previous papers.[20,22,24] Thus, a Li/Li_ySiO_x-C half-cell employing the above mentioned electrolyte has

been characterized by voltammetry (Fig. S5a in the Supplementary Information), impedance spectroscopy (Fig. S5b) and galvanostatic cycling (Fig. S5c and Fig. 5a). The voltammograms of Fig. S5a and the galvanostatic voltage profiles of Fig. S5c reveal a reversible electrochemical process mostly occurring below 1 V. EIS spectra have been recorded at the OCV of the Li/Li$_y$SiO$_x$-C cell as well as after 5 and 10 cycles of voltammetry. The related Nyquist plots of Fig. S5b indicate a stable electrode/electrolyte interface both at the anode and the cathode side, and significant decrease of the cell resistance upon cycling, as confirmed by the results of the NLLS fit[29] reported in Table S2 of the Supplementary Information. Such a suitable impedance response is reflected into reversible operation of the cell, with specific capacity at the steady state of 290 mAh g^{-1} and Coulombic efficiency higher than 99.5% (Fig. 5a). Hence, the Li$_y$SiO$_x$-C/3DG-S cell has been assembled by setting a negative-to-positive ratio (N/P) of 1.07 as represented in in Fig. 5b which reports the voltage vs. specific capacity profiles of the cathode (top x-axes) and the anode (bottom x-axes) performed in lithium half-cell. The shape of the two curves, normalized by taking into account the above N/P ratio, suggests voltage cutoff ranging from 0 to 2.8 V for maximizing the Li$_y$SiO$_x$-C/3DG-S full-cell capacity, and a reasonably restricted range for enabling its cycle life. It is noteworthy that the cell balance in terms of negative-to-positive ratio has a remarkable effect on the cell performance and cycle life.[3] In this work we have assembled the lithium-ion sulfur cell by using only slight excess of the anode capacity (N/P ratio 1.07), as typically performed in the lithium-ion battery in order to achieve high practical capacity and relevant stability. We should however mention that a different N/P ratio, carefully tuned up, may actually vary the lithium-ion sulfur cell voltage, and its delivered capacity. Therefore, a decrease of the N/P ratio can theoretically increase the practical capacity of the cell, however this condition generally leads to a relevant decrease of the cell stability, due to a leak of lithium-ions reservoir by the effect of possible side reaction occurring at the

lithiated anode side during full-cell cycling. In addition, an excessive decrease of the N/P ratio, i.e., to values lower than 1, reflects generally into poor cycling stability, a reduction of the delivered capacity by the cathode side, a decrease of the average cell voltage, and an increase of the cell polarization due to relevant influence of the anode slope on the full-cell profile. In contrast, the raise of the N/P ratio possibly increases the capacity delivered from the cathode, and ensures sufficient lithium ions flow from the anode to the cathode even in presence of side reactions, thus ensuring very stable cycling. However, the latter condition remarkably decreases the practical cell capacity, in which the mass of the anode is taken into account for a proper evaluation of the battery performances.[3]

The novel Li_ySiO_x-C/3DG-S cell, assembled in the charged state due to the electrode configuration, operates upon discharge through the lithium Li_ySiO_x de-alloying reaction at the anode and the conversion to lithium polysulfides at the cathode. Accordingly, the lithium-ion sulfur cell benefits from the multiple-electron reactions and expected low-cost of the electrode materials.[3] Therefore, the study may provide further insight into the electrochemistry of the lithium-ion sulfur battery. The cell has been galvanostatically cycled at a C/5 rate with respect to the cathode mass within 0.8 V and 2.4 V. The first 100 cycles of this cell, reported in Fig. S6 in the Supplementary Information, are considered as a pre-cycling step required in order to achieve the steady-state condition of the cell. During this step the discharge capacity of the cell decreases from about 870, i.e., a value expected by the restricted cutoff, to about 420 and the voltage shape modifies mostly due SEI film formation, and side reactions leading to the variation of the cell balance.[22,24] After few hours of rest, suitable for achieving a further stabilized SEI film at the electrodes surface, the capacity recovers up to 480 mAh g^{-1}, and the cell reveals a remarkably reversible voltage shape (Fig. 5c) reflecting the combination of the anode and cathode profiles (compare with Fig. 5b). Thus, the cell appears characterized by two sloping plateaus upon discharge, respectively

occurring at about 1.9 and 1.3 V, and one voltage plateau upon charge between 1.2 and 2.0 V. Accordingly, the cell operates by an average voltage of 1.5 V, delivering a reversible, steady-state capacity of about 460 mAh g_S^{-1} with a Coulombic efficiency higher than 99% over 200 cycles (Fig. 5d). We have also demonstrated elsewhere[20] remarkable performance by combining a lithiated Si/SiO_x nanosphere anode with dual-type cathode based on a sulfur-activated carbon composite and a catholyte solution, that is, a reversible capacity of 750 mAh g_{sulfur}^{-1} at 1C rate, which was retained by 86% over 500 cycles with a Coulombic efficiency higher than 98%. Both the former and the latter cells have a sulfur mass loading of about 1 mg cm^{-2} (see the Experimental section for further results), respectively leading to areal capacity of about 0.48 mAh cm^{-2} and 0.75 mAh cm^{-2}. Based on the cell voltage and delivered capacity, the Li_ySiO_x-C/3DG-S cell is characterized by a theoretical energy density approaching 700 Wh kg_S^{-1}. Therefore, considering a correction factor of 1/3 that takes into account the contribution of anode, electrolyte and inactive components of typical cells, the estimated practical energy might exceed 220 Wh kg^{-1}, thus suggesting the Li_ySiO_x-C/3DG-S array as a very promising energy-storage system. However, it should be pointed out that the actual energy density of practical batteries is strongly related to the cell design, and technological features.[3]

Figure 5

Conclusions

A sulfur-carbon electrode (3DG-S) was synthesized, characterized and investigated as the cathode in lithium-ion cell in combination with a silicon-oxide, lithium alloying anode (Li_ySiO_x-C). The composite cathode was formed by a three-dimensional framework of randomly-oriented graphene sheets with partially-graphitic structure hosting crystalline sulfur with a loading as high as 65 wt.%, as revealed by diffraction, spectroscopy, and N_2

adsorption and microscopy techniques. The electrochemical investigation in lithium half-cell indicated reactions at 2.3 and 2.0 V upon discharge and at 2.3 and 2.4 V upon charge, according to the reversible redox reaction of sulfur, and low resistance at the electrode/electrolyte interfaces. The electrode delivered large capacity ranging between 1200 and 1000 mAh g_S^{-1} at a current increasing from C/10 to 1C rates, i.e., from 167.5 to 1675 mA g_S^{-1}, respectively, as well as suitable cycling stability with high Coulombic efficiency. The chemically-lithiated Li_ySiO_x-C anode was originally investigated in the same electrolyte solution adopted for the lithium-sulfur cell. The lithium-alloy material delivered with a high efficiency a specific capacity approaching 300 mAh g^{-1} at a voltage lower than 1V, and was therefore considered well suitable electrode for application in lithium-ion sulfur cell. The Li_ySiO_x-C/3DG-S full-cell had a steady-state reversible capacity of about 460 mAh g_S^{-1} and average working voltage of 1.5 V, yielding to a theoretical energy density approaching 700 Wh kg_S^{-1}. The battery reported in this work belongs to a class of full lithium-ion sulfur cells studied in laboratory by systematically varying the features of the electrode and electrolyte components,[20,22,24] in order to explore the a vast range of promising high-energy, Li-metal free, and low-cost battery.

Acknowledgements

This work was performed with the financial support of the Ministerio de Economía y Competitividad (Project MAT2014-59907-R and MAT2017-87541-R) and Junta de Andalucía (Group FQM-175). The work was carried out within the collaboration project "Accordo di Collaborazione Quadro 2015" between the University of Ferrara (Department of Chemical and Pharmaceutical Sciences) and the Sapienza University of Rome (Department of Chemistry), and founded by the grant "Fondo di Ateneo per la Ricerca Locale (FAR) 2017". The authors thank Enrique Rodríguez-Castellón (Dpto. de Química Inorgánica, Cristalografía y Mineralogía, University of Málaga, Spain) for performing X-ray

photoemission spectroscopy (XPS), and Dr. Daniela Palmeri of the Electron Microscopy Centre, Department of Chemical and Pharmaceutical Sciences, University of Ferrara, for recording the electron microscopy.

References

[1] A. Manthiram, Y. Fu, S. Chung, C. Zu, Y. Su, *Chem. Rev.* **2014**, *114*, 11751.

[2] A. Manthiram, Y. Fu, Y.-S. Su, *Acc. Chem. Res.* **2013**, *46*, 1125.

[3] D. Di Lecce, R. Verrelli, J. Hassoun, *Green Chem.* **2017**, *19*, 3442.

[4] L. Carbone, S. G. Greenbaum, J. Hassoun, *Sustain. Energy Fuels* **2017**, *1*, 228.

[5] D. Andre, S. Kim, P. Lamp, F. Lux, F. Maglia, *J. Mater. Chem. A Mater. energy Sustain.* **2015**, *3*, 6709.

[6] R. Demir-Cakan, M. Morcrette, Gangulibabu, A. Guéguen, R. Dedryvère, J.-M. Tarascon, *Energy Environ. Sci.* **2013**, *6*, 176.

[7] Y. V. Mikhaylik, J. R. Akridge, *J. Electrochem. Soc.* **2004**, *151*, A1969.

[8] C. Li, Z. Xi, D. Guo, X. Chen, L. Yin, *Small* **2017**, *1701986*, 1701986.

[9] J. Kim, D. J. Lee, H. G. Jung, Y. K. Sun, J. Hassoun, B. Scrosati, *Adv. Funct. Mater.* **2013**, *23*, 1076.

[10] J. Guo, J. Zhang, F. Jiang, S. Zhao, Q. Su, G. Du, *Electrochim. Acta* **2015**, *176*, 853.

[11] L. Carbone, J. Peng, M. Agostini, M. Gobet, M. Devany, B. Scrosati, S. Greenbaum, J. Hassoun, *ChemElectroChem* **2016**, 1.

[12] X. Wang, Z. Zhang, Y. Qu, Y. Lai, J. Li, *J. Power Sources* **2014**, *256*, 361.

[13] X. Liang, A. Garsuch, L. F. Nazar, *Angew. Chemie - Int. Ed.* **2015**, *54*, 3907.

[14] N. Moreno, A. Caballero, J. Morales, M. Agostini, J. Hassoun, *Mater. Chem. Phys.* **2016**, *180*, 82.

[15] S. Zhang, K. Ueno, K. Dokko, M. Watanabe, *Adv. Energy Mater.* **2015**, *5*, 1500117.

[16] M. Agostini, S. Xiong, A. Matic, J. Hassoun, *Chem. Mater.* **2015**, *27*, 4604.

[17] L. Carbone, T. Coneglian, M. Gobet, S. Munoz, M. Devany, S. Greenbaum, J. Hassoun, *J. Power Sources* **2018**, *377*, 26.

[18] L. Carbone, M. Gobet, J. Peng, M. Devany, B. Scrosati, S. Greenbaum, J. Hassoun, *ACS Appl. Mater. Interfaces* **2015**, *7*, 13859.

[19] M. Agostini, J. Hassoun, *Sci. Rep.* **2015**, *5*, 7591.

[20] S.-K. K. Lee, S.-M. M. Oh, E. Park, B. Scrosati, J. Hassoun, M.-S. S. Park, Y.-J. J. Kim, H. Kim, I. Belharouak, Y.-K. K. Sun, *Nano Lett.* **2015**, *15*, 2863.

[21] F. Jeschull, D. Brandell, K. Edström, M. J. Lacey, *Chem. Commun.* **2015**, *51*, 17100.

[22] M. Agostini, B. Scrosati, J. Hassoun, *Adv. Energy Mater.* **2015**, *5*, 1500481.

[23] S. Thieme, J. Brueckner, A. Meier, I. Bauer, K. Gruber, J. Kaspar, A. Helmer, H. Althues, M. Schmuck, S. Kaskel, *J. Mater. Chem. A* **2015**, *3*, 3808.

[24] M. Agostini, J. Hassoun, J. Liu, M. Jeong, H. Nara, T. Momma, T. Osaka, Y. K. Sun, B. Scrosati, *ACS Appl. Mater. Interfaces* **2014**, *6*, 10924.

[25] Y. Xu, L. Zhao, H. Bai, W. Hong, C. Li, G. Shi, *J. Am. Chem. Soc.* **2009**, *131*, 13490.

[26] H. Chen, C. Wang, W. Dong, W. Lu, Z. Du, L. Chen, *Nano Lett.* **2015**, *15*, 798.

[27] G. A. Elia, J. Hassoun, *ChemElectroChem* **2017**, *4*, 2164.

[28] J. Hassoun, K.-S. Lee, Y.-K. Sun, B. Scrosati, *J. Am. Chem. Soc.* **2011**, *133*, 3139.

[29] B. A. Boukamp, *Solid State Ionics* **1986**, *20*, 31.

[30] T. N. Blanton, D. Majumdar, *Powder Diffr.* **2013**, *28*, 68.

[31] J.-Z. Wang, C. Zhong, S.-L. Chou, H.-K. Liu, *Electrochem. commun.* **2010**, *12*, 1467.

[32] Z.-S. Wu, W. Ren, L. Wen, L. Gao, J. Zhao, Z. Chen, G. Zhou, F. Li, H.-M. Cheng, *ACS Nano* **2010**, *4*, 3187.

[33] O. A. Vargas C., Á. Caballero, J. Morales, *Nanoscale* **2012**, *4*, 2083.

[34] S. Stankovich, D. A. Dikin, R. D. Piner, K. A. Kohlhaas, A. Kleinhammes, Y. Jia, Y. Wu, S. T. Nguyen, R. S. Ruoff, *Carbon N. Y.* **2007**, *45*, 1558.

[35] A. Abouimrane, O. C. Compton, K. Amine, S. T. Nguyen, *J. Phys. Chem. C* **2010**, *114*, 12800.

[36] A. Ganguly, S. Sharma, P. Papakonstantinou, J. Hamilton, *J. Phys. Chem. C* **2011**, *115*, 17009.

[37] S. Abdolhosseinzadeh, H. Asgharzadeh, H. Seop Kim, *Sci. Rep.* **2015**, *5*, 10160.

[38] C. Hernández-Rentero, O. Vargas, A. Caballero, J. Morales, F. Martín, *Electrochim. Acta* **2016**, *222*, 914.

[39] J. Ederer, P. Janoš, P. Ecorchard, J. Tolasz, V. Štengl, H. Beneš, M. Perchacz, O. Pop-Georgievski, *RSC Adv.* **2017**, *7*, 12464.

[40] N. Moreno, A. Caballero, L. Hernán, J. Morales, *Carbon N. Y.* **2014**, *70*, 241.

[41] R. Chen, T. Zhao, J. Lu, F. Wu, L. Li, J. Chen, G. Tan, Y. Ye, K. Amine, *Nano Lett.* **2013**, *13*, 4642.

[42] S. Lu, Y. Cheng, X. Wu, J. Liu, *Nano Lett.* **2013**, *13*, 2485.

[43] B. Ding, C. Yuan, L. Shen, G. Xu, P. Nie, Q. Lai, X. Zhang, *J. Mater. Chem. A* **2013**, *1*, 1096.

[44] Y. Li, Z. Li, Q. Zhang, P. K. Shen, *J. Mater. Chem. A* **2014**, *2*, 4528.

[45] G. Zhou, L. Li, C. Ma, S. Wang, Y. Shi, N. Koratkar, W. Ren, F. Li, H.-M. Cheng, *Nano Energy* **2015**, *11*, 356.

[46] L. Zhong, K. Yang, R. Guan, L. Wang, S. Wang, D. Han, M. Xiao, Y. Meng, *ACS Appl. Mater. Interfaces* **2017**, *9*, 43640.

[47] L. Yan, D. Han, M. Xiao, S. Ren, Y. Li, S. Wang, Y. Meng, *J. Mater. Chem. A* **2017**, *5*, 7015.

[48] J. Hassoun, B. Scrosati, *Angew. Chemie Int. Ed.* **2010**, *49*, 2371.

[49] J. Hassoun, Y. K. Sun, B. Scrosati, *J. Power Sources* **2011**, *196*, 343.

[50] J. Hassoun, J. Kim, D.-J. Lee, H.-G. Jung, S.-M. Lee, Y.-K. Sun, B. Scrosati, *J. Power*

Sources **2012**, *202*, 308.

[51] N. Moreno, M. Agostini, A. Caballero, J. Morales, J. Hassoun, *Chem. Commun.* **2015**, *51*, 14540.

Table captions

Table 1. Contribution of the different components used in the fitting of the C 1s photoemission peak (%) in the XPS spectra of GO (Fig. 2c) and 3DG (Fig. 2d). See experimental section for sample's acronym.

Table 2. Textural properties of GO and 3DG obtained N_2 by the DFT modelling of the adsorption/desorption isotherms GO and 3DG samples (Fig. 2e,f). See experimental section for sample's acronym.

Figure captions

Figure 1. Schematic representation of the lithium-ion sulfur cell studied in this work

Figure 2. (a) XRD patterns of GO (orange), 3DG (green) and 3DG-S composite (red). **(b)** Raman spectra of GO (orange) and 3DG (green). **(c,d)** XPS spectra for the C 1s photoemission peak of the **(c)** GO and **(d)** 3DG samples. **(e)** N_2 adsorption/desorption isotherms and **(f)** pore size distribution calculated by the DFT model for GO (orange) and 3DG (green) samples. See experimental section for sample's acronym.

Figure 3. SEM images at various magnifications for **(a,b)** GO, **(c,e,g)** 3DG and **(d,f,h)** 3DG-S. **(i)** SEM image and related SEM-EDX elemental maps of **(l)** C and **(m)** S for the 3DG-S composite. See experimental section for sample's acronym.

Figure 4. Electrochemical performance of the 3DG-S composite in lithium cell with DOL:DME (1:1 w/w), 1 mol kg^{-1} LiTFSI, 1 mol kg^{-1} $LiNO_3$ electrolyte. See experimental section for electrolyte identification **(a)** Cyclic voltammetry profiles within the 1.8 – 2.8 V range with a scan rate of 0.1 mV s^{-1} (see Fig. S2 in the Supplementary Information reporting the results of EIS tests performed during the voltammetry test). **(b)** Rate capability test in lithium half-cell in terms of cycling behavior at C/10, C/8, C/5, C/3, C/2, and 1C rates (1C = 1675 mA g_S^{-1}; specific capacity on the left y-axis and Coulombic efficiency on the right y-

axis; see Fig. S3 in the Supplementary Information for the related voltage profiles). **(c)** Galvanostatic cycling tests in lithium half-cell at C/3, C/2, and 1C rates (1C = 1675 mA g_S^{-1}) in terms of **(c)** voltage profiles and **(d)** cycling behavior over 100 cycles (specific capacity on the left y-axis and Coulombic efficiency on the right y-axis). Sulfur loading between 1.4 – 2.2 mg cm^{-2}. Cycling tests performed within the 1.8 – 2.8 V voltage range for the 1C rate, and the 1.9 – 2.8 V range for all the other C-rates.

Figure 5. (a) Galvanostatic cycling behavior of the Li_ySiO_x-C electrode in lithium half-cell with DOL:DME (1:1 w/w), 1 mol kg^{-1} LiTFSI, 1 mol kg^{-1} $LiNO_3$ electrolyte at 100 mA g^{-1} within the 0.01 – 2.0 V voltage range (specific capacity on the left y-axis and Coulombic efficiency on the right y-axis; see Fig. S5 in the Supplementary Information reporting the related voltage profiles as well as further electrochemical tests on the Li_ySiO_x-C electrode). **(b)** Comparison of the voltage profiles related to Li/Li_ySiO_x-C and Li/3DG-S half-cells using the DOL:DME (1:1 v/v), 1 mol kg^{-1} LiTFSI, 1 mol kg^{-1} $LiNO_3$ electrolyte, respectively cycled at 100 and 560 mA g^{-1} within the 0.01 – 2.0 and 1.9 – 2.8 V voltage ranges; the chart reflects the Li_ySiO_x-C/3DG-S cell balance (P/N ratio), whereas the specific capacities (top and down side x-axes) are normalized to the corresponding active material mass loadings. **(c-d)** Galvanostatic test of the Li_ySiO_x-C/3DG-S full-cell at a C/5 rate with respect to the cathode mass (1C = 1675 mA g_S^{-1}) within the 0.8 V – 2.4 V voltage range in terms of **(c)** voltage profiles and **(d)** cycling behavior over 200 cycles (specific capacity on the left y-axis and Coulombic efficiency on the right y-axis).

Samples	C-C	C-O alkox	C-O epox	C=O carbonyl	C-O carboxyl	$\pi \rightarrow \pi^*$
BE (eV)	*284.8*	*285.9*	*286.7*	*288.0*	*289.0*	*290.8*
GO	38.12	--	50.97	7.69	3.22	-
3DG	64.23	7.30	7.30	6.02	4.08	4.25

Table 1

Samples	S_{BET} ($m^2 \cdot g^{-1}$)	V_T ($cm^3 \cdot g^{-1}$)
GO	52	0.06
3DG	348	0.38

Table 2

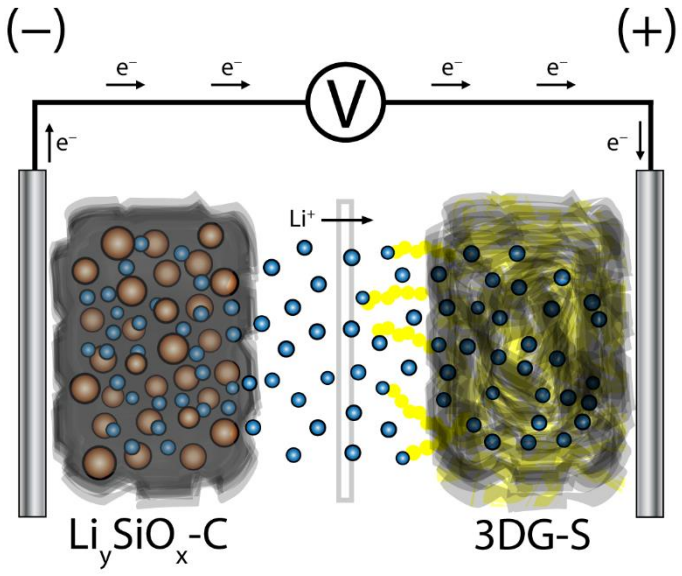

Figure 1

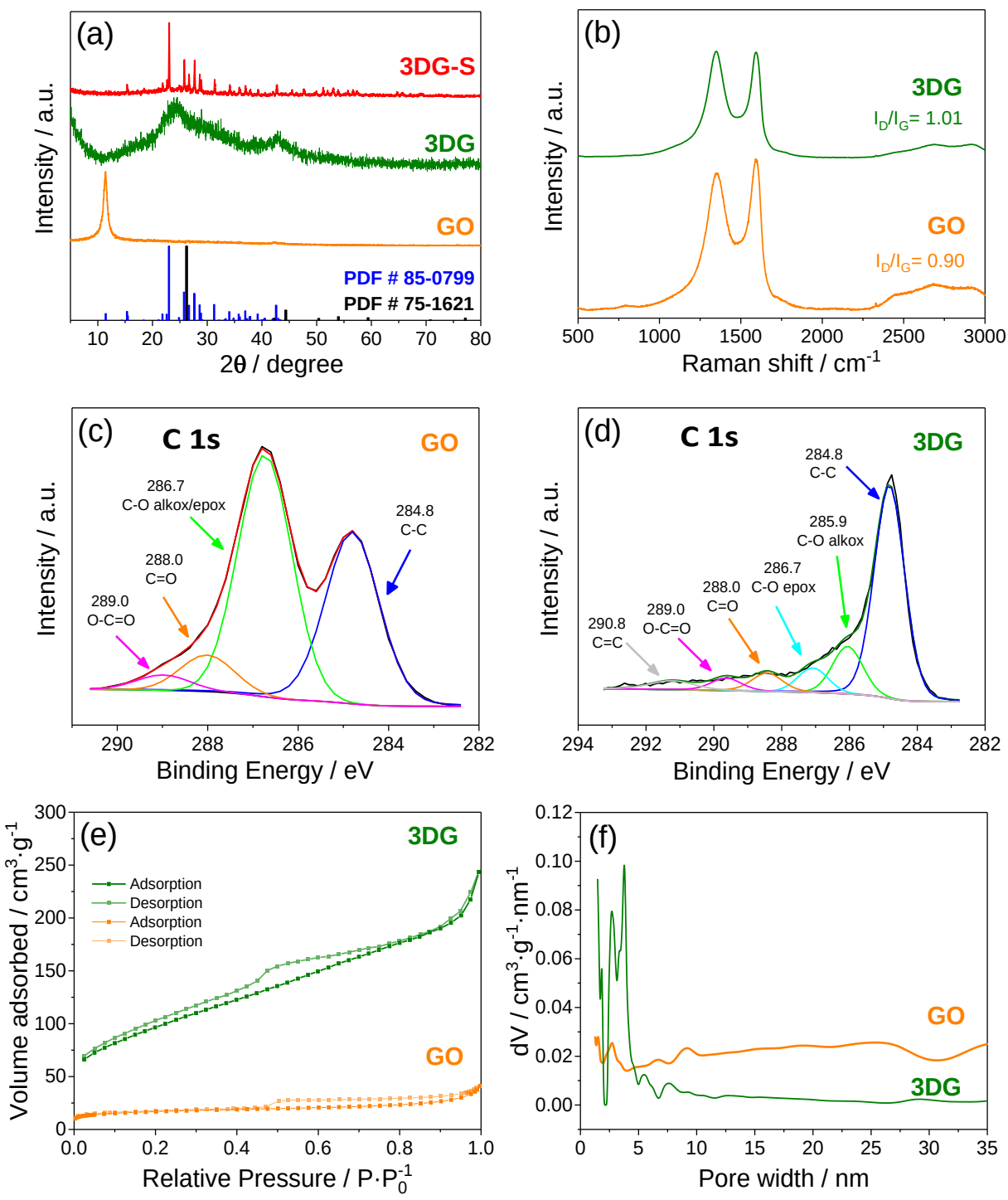
(a)
3DG-S
3DG
GO
PDF # 85-0799
PDF # 75-1621
Intensity / a.u.
2θ / degree
(b)
3DG
I_D/I_G= 1.01
GO
I_D/I_G= 0.90
Intensity / a.u.
Raman shift / cm-1
(c)
C 1s
GO
286.7
C-O alkox/epox
288.0
C=O
289.0
O-C=O
284.8
C-C
Intensity / a.u.
Binding Energy / eV
(d)
C 1s
3DG
284.8
C-C
285.9
C-O alkox
286.7
C-O epox
288.0
C=O
289.0
O-C=O
290.8
C=C
Intensity / a.u.
Binding Energy / eV
(e)
3DG
Adsorption
Desorption
Adsorption
Desorption
GO
Volume adsorbed / cm3·g-1
Relative Pressure / P·P0-1
(f)
GO
3DG
dV / cm3·g-1·nm-1
Pore width / nm

Figure 2

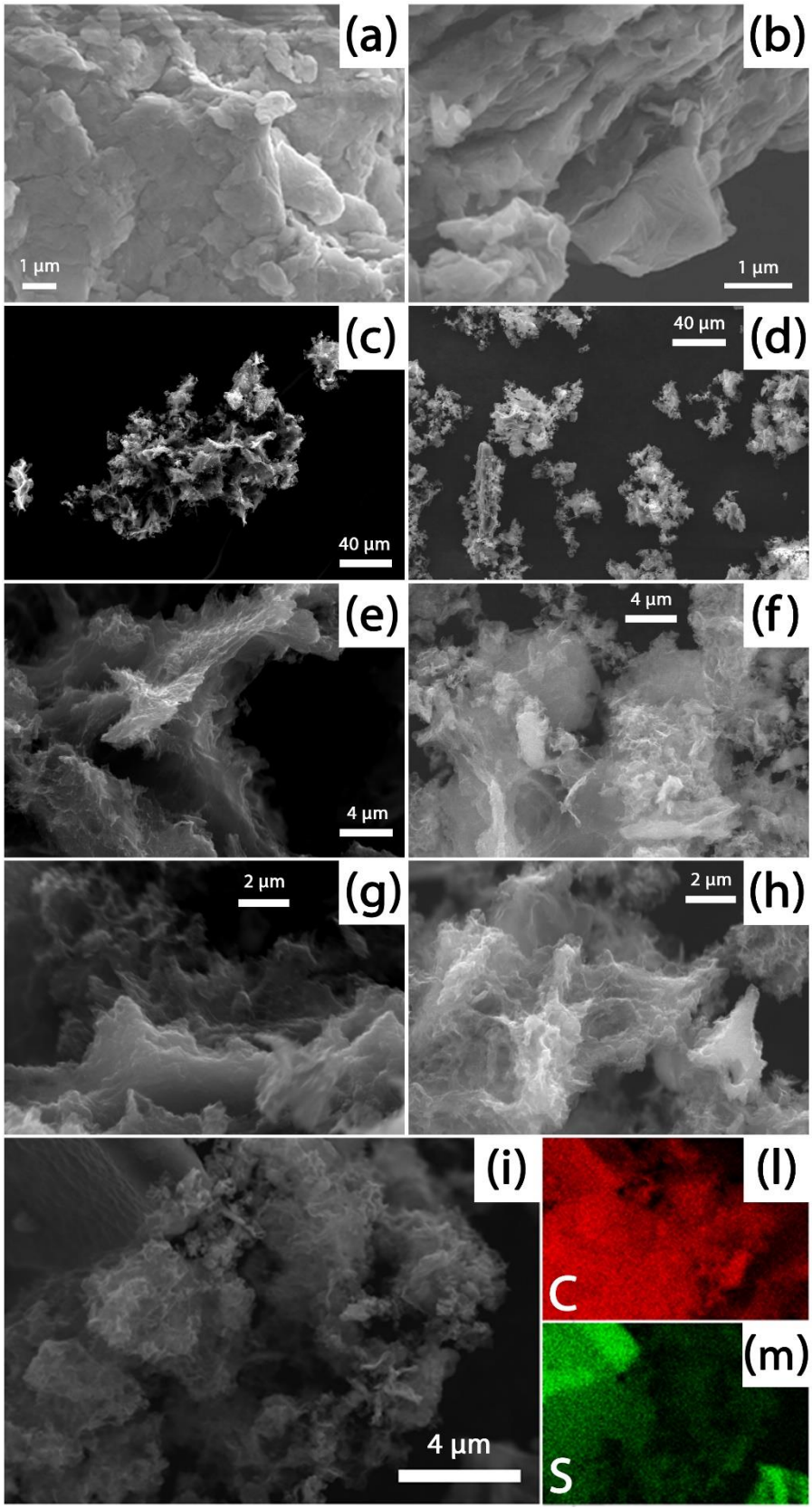

Figure 3

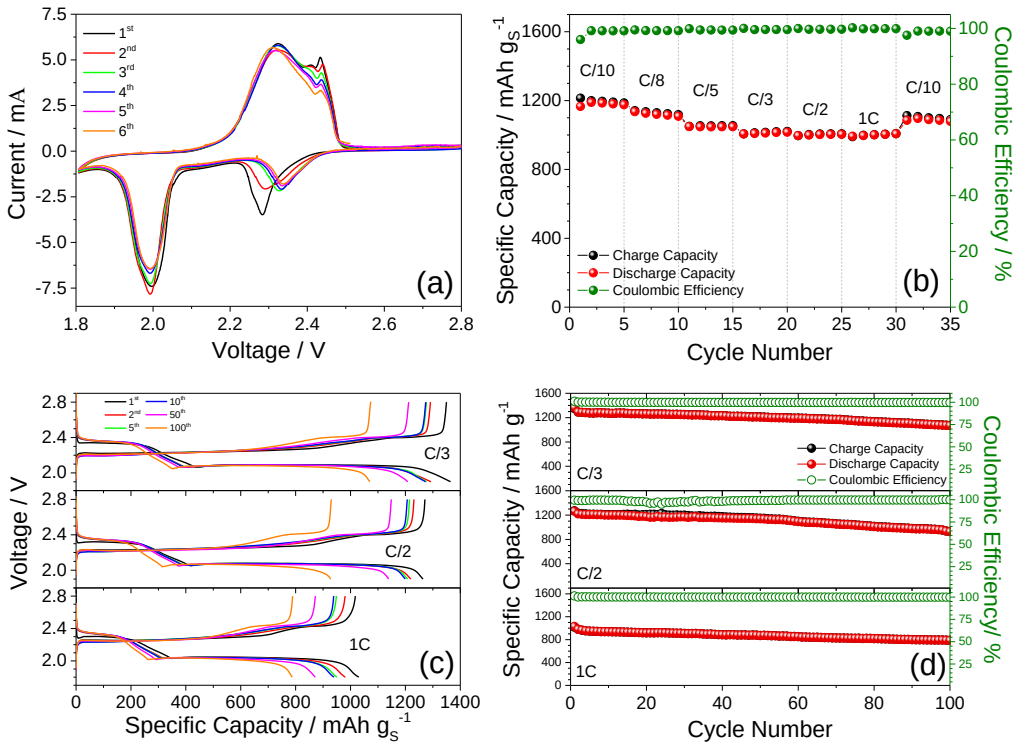
Current / mA
Voltage / V
1st
2nd
3rd
4th
5th
6th
(a)
Specific Capacity / mAh gS-1
Coulombic Efficiency / %
Cycle Number
C/10
C/8
C/5
C/3
C/2
1C
C/10
Charge Capacity
Discharge Capacity
Coulombic Efficiency
(b)
Voltage / V
1st
2nd
5th
10th
50th
100th
C/3
C/2
1C
(c)
Specific Capacity / mAh gS-1
Specific Capacity / mAh g-1
Coulombic Efficiency/ %
Cycle Number
Charge Capacity
Discharge Capacity
Coulombic Efficiency
C/3
C/2
1C
(d)

Figure 4

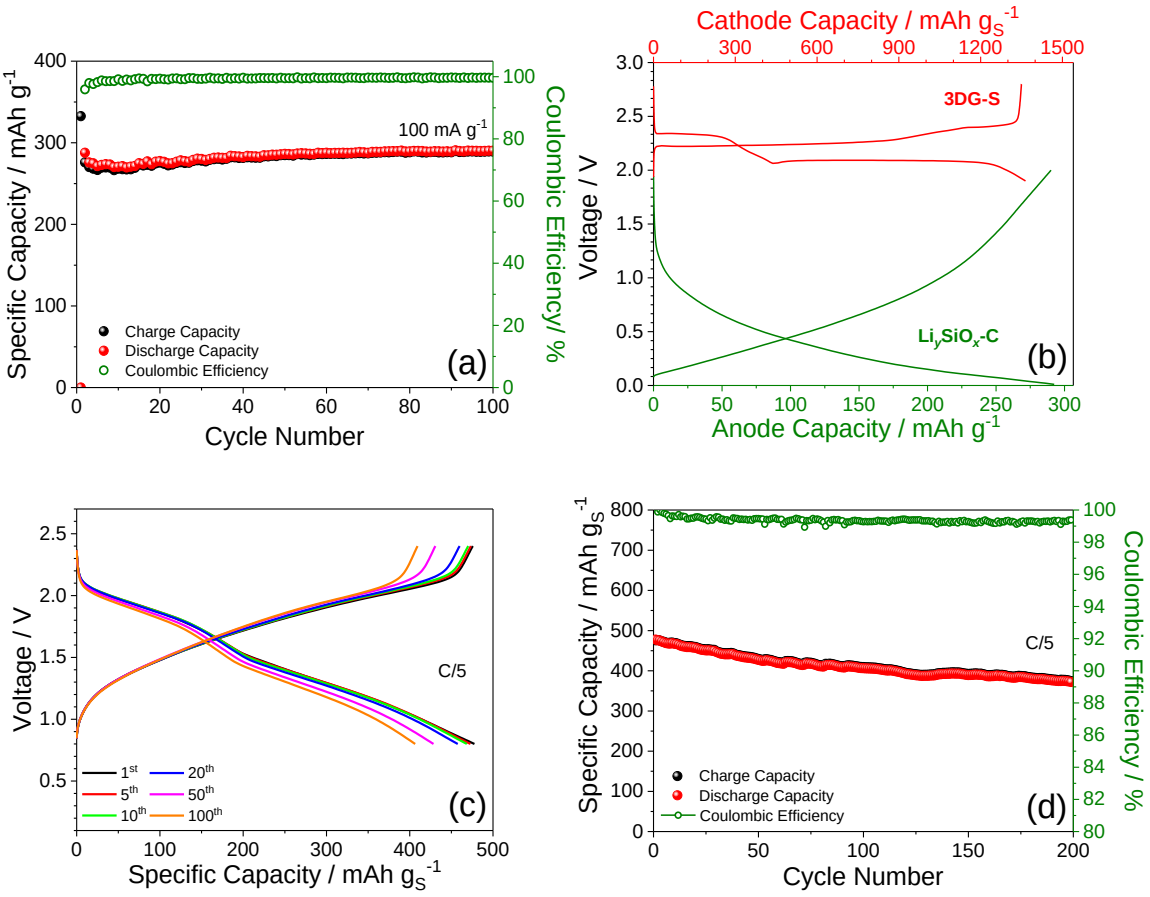
Specific Capacity / mAh g-1
Coulombic Efficiency/ %
Cycle Number
100 mA g-1
Charge Capacity
Discharge Capacity
Coulombic Efficiency
(a)
Cathode Capacity / mAh gS-1
Voltage / V
Anode Capacity / mAh g-1
3DG-S
LiySiOx-C
(b)
Voltage / V
Specific Capacity / mAh gS-1
C/5
1st
20th
5th
50th
10th
100th
(c)
Specific Capacity / mAh gS-1
Coulombic Efficiency / %
Cycle Number
C/5
Charge Capacity
Discharge Capacity
Coulombic Efficiency
(d)

Figure 5

Table of content